



# Effects of *Ti6Al4V* mechanical and thermal surface modification on the adhesion of a chitosan-bioactive glass coating

Michela Sanguedolce<sup>1</sup> · Giovanna Rotella<sup>2</sup> · Federica Curcio<sup>3</sup> · Riccardo Pelaccia<sup>4</sup> · Vincenzina Siciliani<sup>4</sup> · Roberta Cassano<sup>3</sup> · Leonardo Orazi<sup>4</sup> · Luigino Filice<sup>1</sup>

Received: 21 October 2022 / Accepted: 16 January 2023 / Published online: 8 February 2023  
© The Author(s) 2023

## Abstract

Biomedical implants interact with human tissues introducing significant perturbation into the body. Implant surfaces can be then functionalized enabling better biocompatibility. At the same time, the additional use of a coating provides further functions such as corrosion protection, osteointegration, and drug delivery. In this context, a composite made of chitosan and bioactive glass nanoparticles has been used for coating *Ti6Al4V* alloy samples processed beforehand using different processes, i.e., polishing, milling, grit blasting, and electrical discharge machining. Experiments have been carried out to correlate substrate surface conditions and coating effectiveness in terms of scratch resistance with the final aim to obtain suitable guidelines to improve substrate-coating performances.

**Keywords** Titanium · Surface modification · Surface integrity · Coating adhesion · Chitosan · Bioactive glass

## 1 Introduction

Metals play a main role in the framework of biomaterials as most implants contain at least one metallic part. In particular, metallic biomaterials employed for orthopedic applications consist of titanium alloys, stainless steel, and Co-Cr-Mo alloys: the first two groups are widely employed for fracture fixation devices such as plates, screws, nails, and wires. Notably, such components are mostly made from titanium alloys since this class of materials possesses high biocompatibility, low infection risk, fatigue strength, and corrosion resistance and allows broken bones to be firmly

stabilized avoiding micro-movements under the influence of considerable forces [1].

Biomaterial-tissue interactions largely affect implant operation and, eventually, its failure as these are related to the alteration of physiological processes. Many factors contribute to implant success: not only implant material and its surface properties are involved but also device design, mechanical properties (i.e., stiffness), implantation site, and surgical procedure [2].

Focusing on surface characteristics and local stiffness, there is the scope for action to impact in a meaningful way on implant behavior with respect to the body environment, in particular tissue-implant interaction. The deposition of a coating represents an effective way to modify the superficial layers of a device without affecting its bulk. Chitosan-based materials, known for their good osteogenic and drug delivery properties, are being thoroughly investigated to improve implant bioactivity, antibacterial activity but also the protection of metallic parts from corrosion phenomena [3, 4].

However, pure chitosan has poor mechanical properties and its adhesion on metal substrates is considered weak in terms of bond interactions [5]. As an example, chitosan coating has been tested on stainless steel fixation screws simulating screw placement into bone, showing promising results but the necessity of coating retention improvement [6]. Creating chitosan/bioactive glass (BG) composites represents

✉ Michela Sanguedolce  
michela.sanguedolce@unical.it

<sup>1</sup> Department of Mechanical, Energy and Management Engineering, University of Calabria, Via P. Bucci Cubo 45C, 87036 Rende, CS, Italy

<sup>2</sup> Department of Management, Finance and Technology, LUM University, S.S. 100 Km 18, 70010 Casamassima, BA, Italy

<sup>3</sup> Department of Pharmacy, Health, and Nutritional Sciences, University of Calabria, Via P. Bucci, 87036 Rende, CS, Italy

<sup>4</sup> Department of Science and Methods for Engineering, University of Modena and Reggio Emilia, Via Amendola 2, 42122 Reggio Emilia, RE, Italy

a viable solution, as BG can be employed for both bonding osteogenesis and mechanical properties improvement [7]. At the same time, the tuning of the substrate properties [8], as altering the surface chemical composition, wettability, and mechanical adhesion, might significantly improve the system-coating performances in all aforementioned aspects.

In implants and bone fixator manufacturing chains, typical secondary processes involve milling to obtain the final desired shape [9], while grinding, polishing, and sandblasting are used to tune surface features [2]. Techniques such as electrical discharge machining [10] and laser treatment [11] are becoming part of the surface modification phase due to the peculiar topographical, microstructural, and compositional properties that can be conveyed to the part. Furthermore, cryogenic treatment, as a complement to traditional heat treatment, has been subject of increasing interest due to improvements in surface integrity and corrosion resistance [12].

The processes investigated in this work, namely, polishing, milling, grit-blasting, and electrical discharge machining, involve a wide range of surface modification mechanisms [13], and then, each one of them possesses its peculiarities in terms of surface features, based on processing parameters. This experimental campaign has the objective to critically identify how different textures affect chitosan-based coating adhesion as previous works do not highlight a systematic study of correlation between texture parameters and adhesion. The guiding principle is to improve the adhesion of a chitosan/bioglass coating and simultaneously provide a comprehensive overview of how processing affects metallic *Ti6Al4V* substrate by studying substrate surface integrity and wettability and by evaluating coating scratch resistance.

## 2 Materials and methods

### 2.1 Metallic substrate processing

The substrates employed for the experimental campaign are *Ti6Al4V* discs of 20 mm diameter and 5 mm thickness, obtained from a round bar of which microstructure consists of  $\alpha$  equiaxed grains with intergranular  $\beta$ . Four preparation processes were studied, namely, polishing (P), face milling (M), grit-blasting (GB), and electrical discharge machining (EDM). All samples have been previously ground and polished up to 0.5  $\mu\text{m}$  grade to ensure the same preliminary preparation before further processing. The face milling process has been conducted on a CNC vertical machining center, employing a carbide milling cutter coated with *TiAlSiN*, 16 mm diameter (Meusburger Georg GmbH & Co KG, Austria). Milling parameters have been chosen as suggested by the manufacturer: cutting speed 60 m/min, feed rate 250 mm/min, depth of

cut 0.1 mm, and flood lubrication. Alumina particles (F36 grit size) have been used for grit blasting performing two passes of 10 s each, with a 90° angle. Air pressure was set to 0.3 MPa [14], while the sample-nozzle distance was set to 60 mm. For EDM, a die sinking process was selected, using a flat copper electrode and a commercial dielectric fluid specific for EDM (Electroflux TE), side flushing. According to preliminary tests, manufacturer's advice, and literature [15], pulse duration (tON) and pulse interval (tOFF) were set respectively equal to 25  $\mu\text{s}$  and 16  $\mu\text{s}$ , while a voltage of 135 V was employed, reaching a discharge current up to 2 A.

### 2.2 Characterization of substrates

Each type of processed substrate was cut perpendicularly to the treated face, embedded on a black bakelite mounting resin, and mechanically polished up to 0.5  $\mu\text{m}$  grade. Nanohardness has been measured through the depth (10 replications for each depth value) to assess the variations generated by the processes through a NH<sup>2</sup> CSM Nanoindentation Platform (Anton Paar GmbH, Austria) equipped with a Berkovich diamond tip. Indentations were performed at a maximum load of 50 mN with 10 s of dwell time [8, 16]. For microstructural analysis, the polished samples have been etched employing Kroll's reagent and analyzed through an optical microscope.

Furthermore, a Confovis structured light profilometer connected to a Nikon Eclipse LV150N microscope was employed to obtain real surface topography parameters (scanned area size: 0.5 mm  $\times$  0.5 mm, four replications). Additionally, the images of the non-sectioned surfaces were taken using a scanning electron microscope (ESEM Quanta-200 — Fei Oxford Instruments), equipped with the detector for EDS analysis (X-EDS Oxford INCA-350), which was performed on different areas of the samples (area size: 400  $\mu\text{m}$   $\times$  520  $\mu\text{m}$ ) to confirm the surfaces' composition. In addition, the EDS analysis was combined with  $\mu$ Raman spectroscopy (LabRam — Jobin–Yvon) employing a 532-nm wavelength and 40-mW power laser.

Contact angle (CA) was quantified employing the sessile drop technique (DSA30S — Krüss Scientific, Germany): drops of 1  $\mu\text{l}$  of chitosan/bioglass solution used for coating and described in paragraph 2.3 were delivered on substrate surfaces performing five repetitions for each sample over a time interval of 300 s. For milled surfaces, due to topography anisotropy, five measurements were made for each of the two directions: direction 1 (D1) and direction 2 (D2) parallel and orthogonal to the machining direction, respectively.

### 2.3 Chitosan/bioglass coating preparation and deposition

A 0.7% solution of chitosan (CS — medium molecular weight, 75–85% degree of deacetylation) in 1% acetic acid was prepared. The solution was kept under magnetic stirring

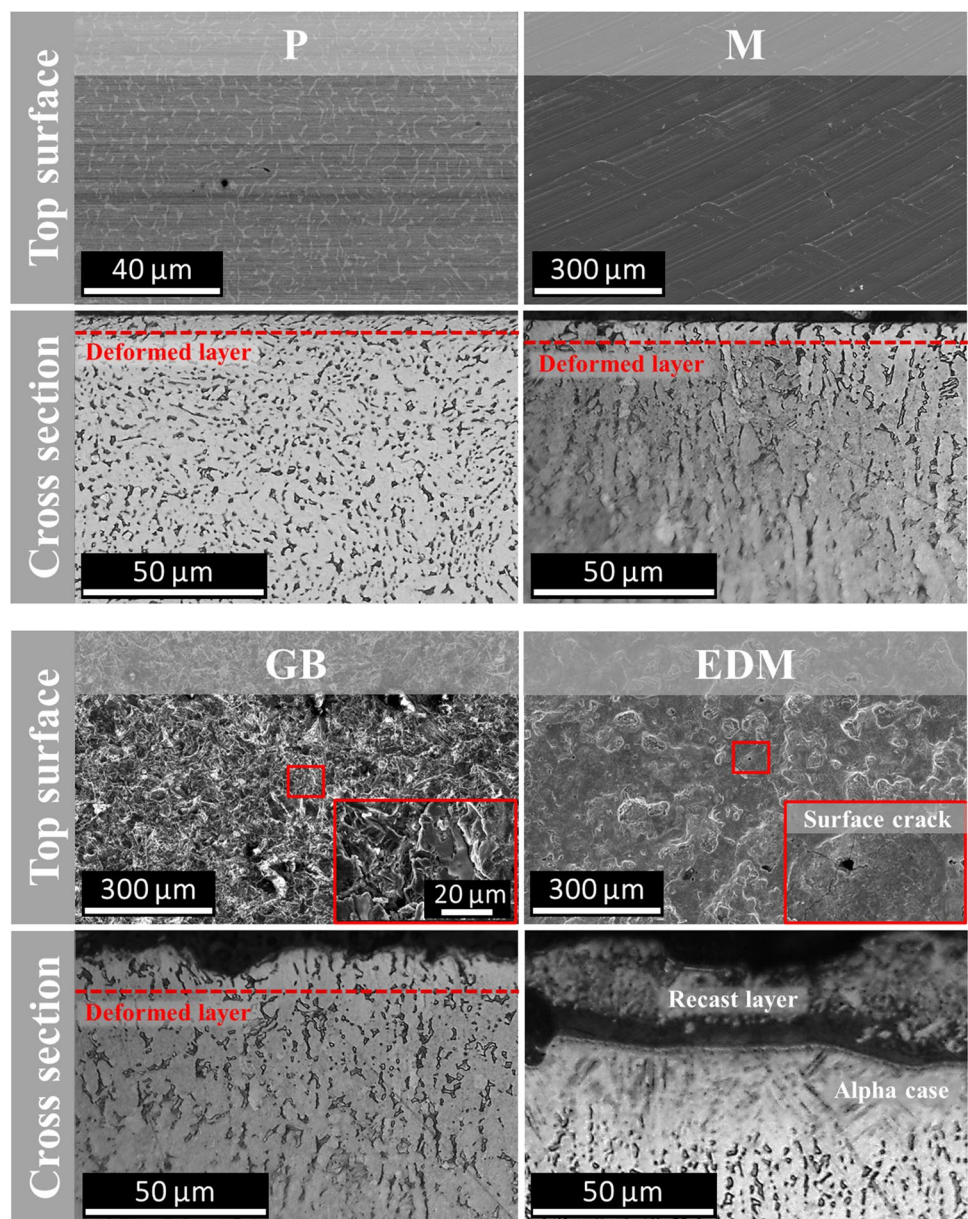
in an oil bath, at 40 °C overnight [17]. It was then centrifuged, adding to the supernatant 0.3% of bioactive glass nanoparticles (nBG — 77 wt% SiO<sub>2</sub>, 14 wt% CaO, 9 wt% P<sub>2</sub>O<sub>5</sub>, particle size below 100 nm). The mixture was kept under agitation overnight and then sonicated at 40 °C for 20 min [18]. Two milliliters of solution was used to coat each *Ti6Al4V* support by the solution casting method. Substrates were previously sonicated in distilled water and ethanol bath for 15 min, for 3 times respectively. The coated discs were then dried in an oven at 80 °C for 7 h [19].

### 2.4 Adhesion tests

Adhesion tests have been performed utilizing a micro-scratch tester (Anton Paar GmbH, Austria) through a Rockwell C tip

(120°, 100 μm radius). Scratch testing, although qualitative, is considered an advantageous test means relating to usage conditions, in particular for orthopedic implants [20]. Coatings have been tested in a controlled laboratory environment (25 °C temperature, 60% relative humidity). Each type of sample, that is polished (P), face milled (M), grit blasted (GB), and EDM treated (EDM) coated with chitosan/bioactive glass nanoparticles (CS + nBG), has been replicated three times to ensure statistical robustness. A number of 10 scratches, spaced at least by 5 times the scratch width, has been performed on each sample. The parameter selection was supported by a thorough campaign of preliminary tests, following ASTM D7027-20 [21] guidelines and literature. A linearly increasing load from 10 to 5000 mN has been applied, along a distance of 2 mm with a displacement rate

**Fig. 1** Images of *Ti6Al4V* substrates after processing: SEM images of the worked surface in the top rows and micrographs of cross-sectioned and etched samples in the bottom rows



of 10  $\mu\text{m/s}$  [22]. Scratches have been analyzed employing an optical microscope and a SEM ZEISS Crossbeam 350, to identify different failure mechanisms and critical loads with corresponding penetration depth from computed scratch curves. Average coating thickness has been estimated employing an average penetration depth value, corresponding to curve flattening as the tip reaches the substrate.

### 3 Results

#### 3.1 Substrates characterization

Processing of samples, as expected, brought a wide range of surface modification mechanisms as seen in the top row of Fig. 1 showing processed surface (magnifications in red rectangles).

The microstructure of the P, M, and GB samples is unchanged with  $\alpha$  equiaxed grains and intergranular  $\beta$ . Surface grain distortion distinctive of the plastic deformation processes is highlighted with dotted lines in Fig. 1 of cross-sectioned P, M, and GB samples.

The significant cold working after the face milling process is confirmed by the nano-hardness profile, reaching values up to 5.8 GPa below the surface. The hardness profile for P and GB samples is nearly unaffected, except

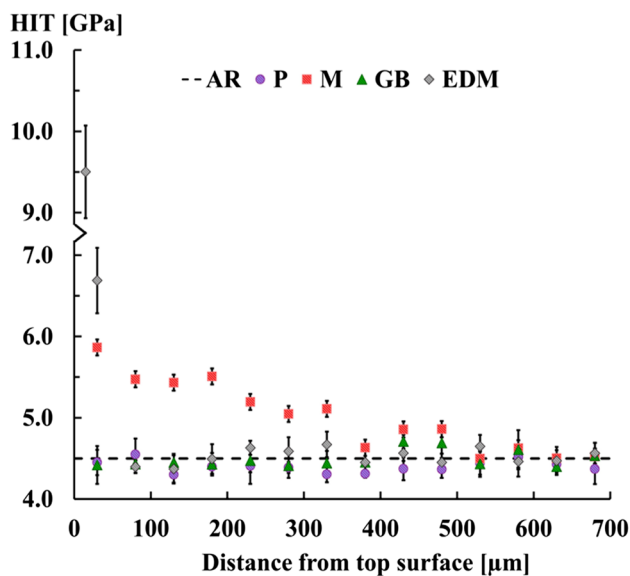


Fig. 2 Nano-hardness profiles of *Ti6Al4V* substrates after processing, compared to as received (AR) conditions. Reported error bars represent the standard deviation

for a few  $\mu\text{m}$  thick layer, not detected by the instrument (Fig. 2) although the deformed portion of GB being larger.

Fig. 3 SEM image of *Ti6Al4V* after EDM processing: cross-section of the substrate with subsurface cracks

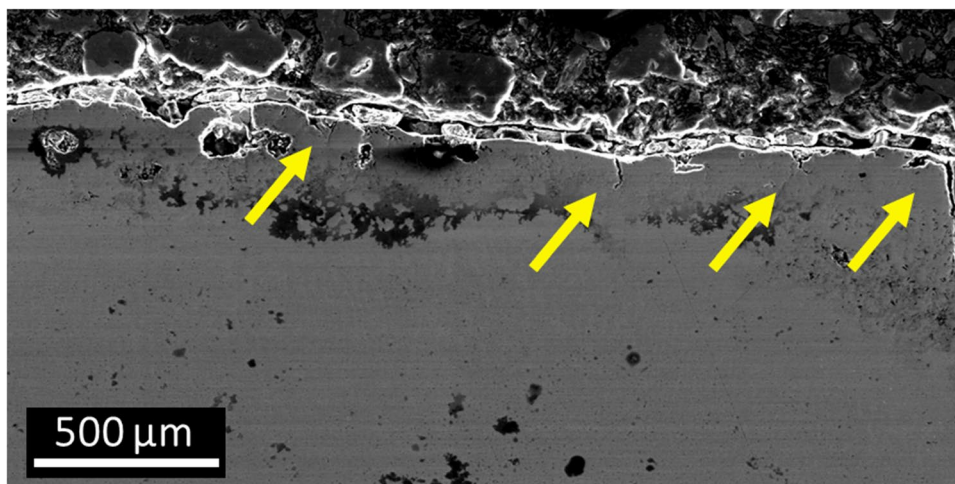
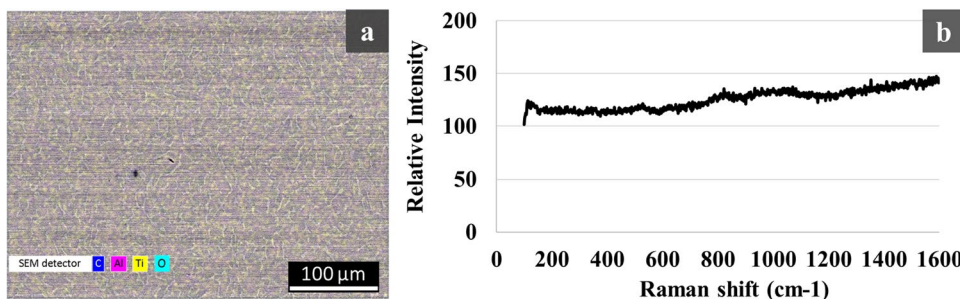
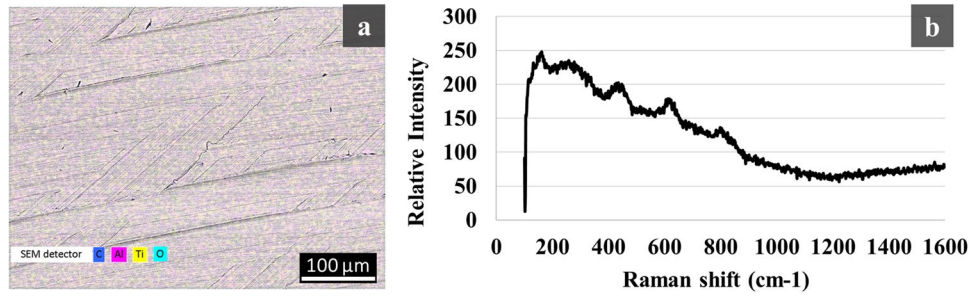


Fig. 4 Polished *Ti6Al4V* surface: a EDS mapping, b Raman spectra



**Fig. 5** Milled *Ti6Al4V* surface: **a** EDS mapping, **b** Raman spectra



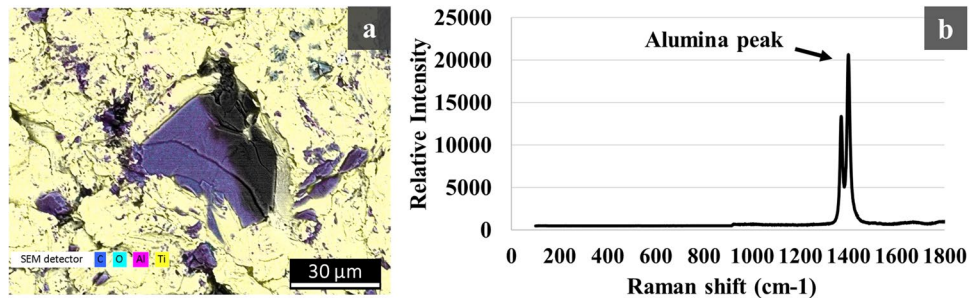
Concerning EDM samples, the formation of a thick recast layer of hard and fragile titanium oxide with an average thickness of  $19.0 \pm 2.9 \mu\text{m}$  was detected. A transformation zone (alpha case) is confirmed by the presence of acicular alpha and the layer has an average thickness of  $16.8 \pm 1.4 \mu\text{m}$ . The presence of surface and subsurface cracks is recognizable in the rectangle magnification in Figs. 1 and 3 as pointed by the arrows.

The combination of EDS analysis and  $\mu\text{Raman}$  spectroscopy was used to better assess the surface of the samples in terms of chemical alteration and oxides formation. More in detail, Figs. 4, 5, 6, and 7 show the analysis in areas of interest of samples P, M, GB, and EDM, respectively. The EDS mapping of polished sample displays, as expected, a negligible presence of oxygen and, connected to this result, the Raman spectrum shows no signal, thus evidencing the absence of rutile titanium dioxide [23]. The same results were obtained for milled surface.

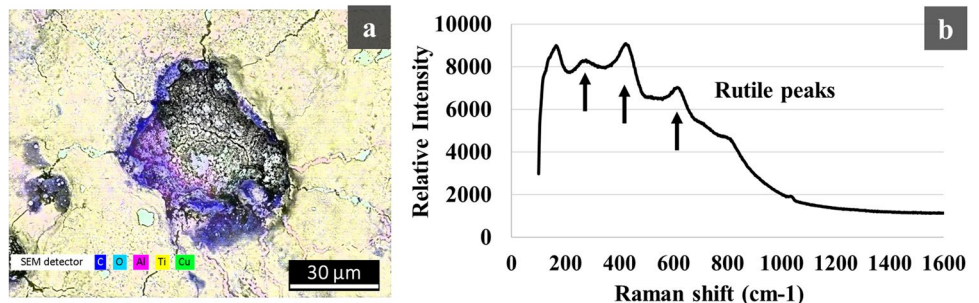
Instead, from EDS mapping of the GB sample, a great amount of oxygen was detected (Fig. 6a), confirmed by the Raman spectrum with the peak of alumina [24, 25], an oxide present in the sample as a processing residue. To confirm this, it is worth noting that the percentage of aluminum in the grit-blasted sample was doubled in relation to the standard value for *Ti6Al4V* obtained in both polished and milled ones. From EDS mapping of the EDM-treated surface (Fig. 7b), copper and oxygen residuals have been detected because of tool-electrode material and rapid oxidation on contact with air, respectively. The Raman spectrum detected the three peaks of rutile in good agreement with the findings of the literature about the characterization of the recast layer of titanium samples processed with EDM [26].

Surface morphology after sample processing is shown in Fig. 8, and the main parameters are reported in Table 1. As reasonably expected, the lowest and most regular

**Fig. 6** Grit-blasted *Ti6Al4V* surface: **a** EDS mapping, **b** Raman spectra



**Fig. 7** EDM treated *Ti6Al4V* surface: **a** EDS mapping, **b** Raman spectra



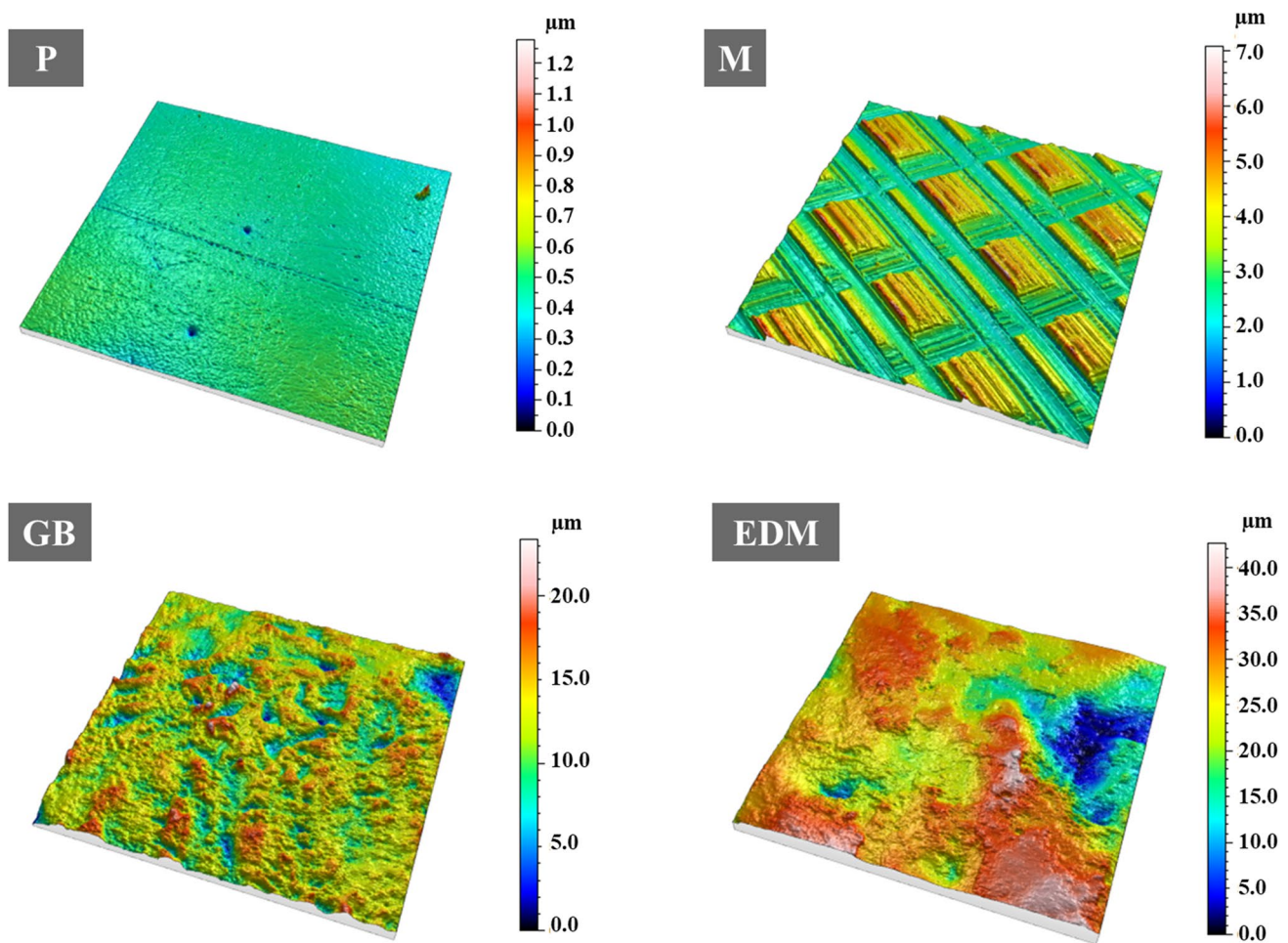


**Fig. 8** Surface roughness distribution for processed *Ti6Al4V* samples, scanned area size: 0.5 mm × 0.5 mm

distribution is found for polished ones, followed by the grid-like texture for milling. Surface unevenness finds a maximum for EDM-treated surfaces, together with the highest maximum height. The high standard deviation found for polished surface in terms of  $S_z$ ,  $S_{ku}$ , and  $S_{kk}$  depended by random imperfections and notched areas that strongly influenced their calculation. On the contrary, the values of  $S_a$  and  $S_q$ , less influenced by these random imperfections, showed acceptable standard deviation, confirming the regular distribution and the low roughness of the polished surface.

Regarding the contact angle (Fig. 9), the lowest value was found for GB samples, obtaining  $26^\circ$  at time 0 s, decreasing up to  $12^\circ$  after 300 s. P and EDM samples show comparable values,  $50^\circ$  and  $53^\circ$  at time 0 s, respectively, at 300 s contact angle settles to around  $30^\circ$  for both. The lowest wettability was found for M samples, showing contact angles above  $60^\circ$  at time 0 s and above  $42^\circ$  at time 300 s in the direction parallel to tool passes (D1); values further increased in the direction orthogonal to tool passes (D2).

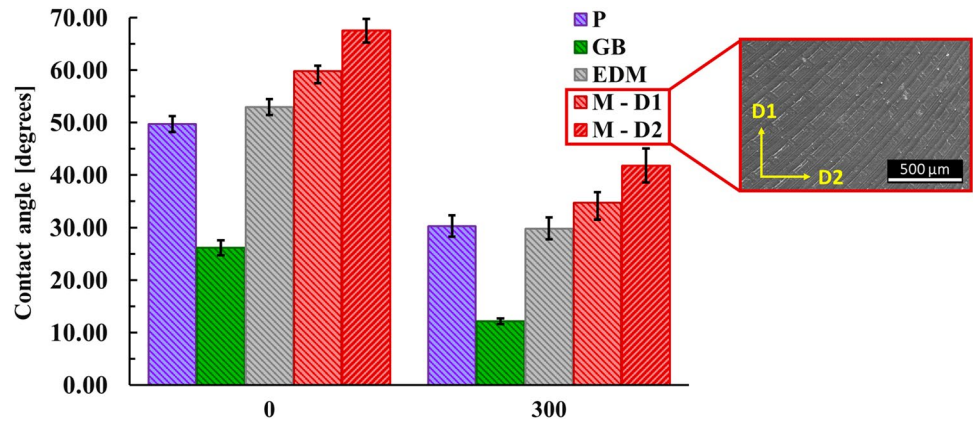
### 3.2 Coating adhesion

Coating failure mechanisms are the same, apart from variations in critical loads: (i) initial plastic deformation and plowing; (ii) cohesive failure, showing transversal and longitudinal cracks which interconnect at a critical load; (iii) adhesive failure, with formerly surface

**Table 1** Surface roughness parameters for processed samples — height parameters following ISO 25178:  $S_a$  arithmetical mean height,  $S_z$  maximum height,  $S_q$  root-mean-square height,  $S_{sk}$  skewness,  $S_{ku}$  kurtosis. The standard deviation is reported in parentheses

Roughness parameter	P	M	GB	EDM
$S_a$ ( $\mu\text{m}$ )	0.05 (0.01)	0.68 (0.04)	2.26 (0.16)	5.97 (1.09)
$S_z$ ( $\mu\text{m}$ )	1.51 (0.79)	6.82 (0.37)	26.72 (1.21)	46.12 (5.67)
$S_q$ ( $\mu\text{m}$ )	0.06 (0.01)	0.80 (0.04)	2.95 (0.18)	7.47 (1.28)
$S_{sk}$ (—)	−0.32 (0.66)	0.80 (0.07)	−0.45 (0.17)	−0.58 (0.40)
$S_{ku}$ (—)	11.18 (12.18)	2.22 (1.00)	3.91 (0.19)	3.27 (0.85)

**Fig. 9** Chitosan/bioglass solution contact angle for treated surfaces measured in a controlled laboratory environment (25 °C temperature, 60% relative humidity). Reported error bars represent the standard deviation

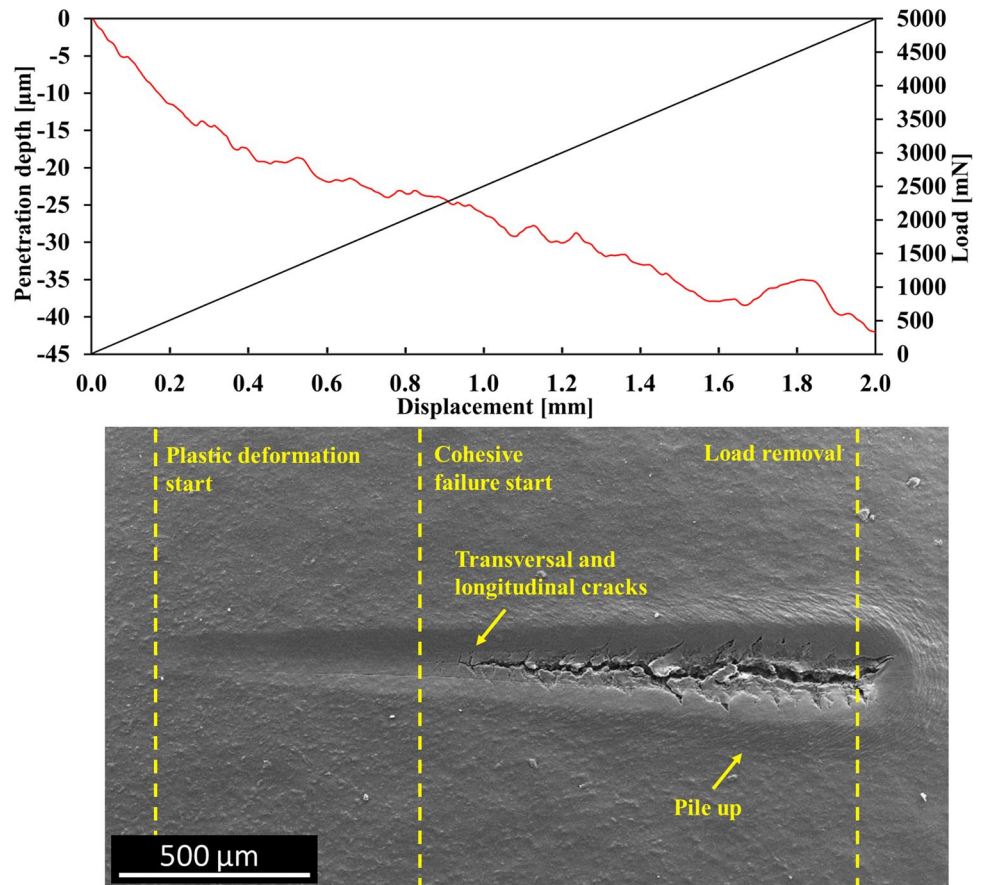


cracks reaching the substrate and complete detachment of the coating. An example of results from a scratch test is reported in Fig. 10, showing the pile-up phenomenon from the onset of plastic deformation to the end of the scratch from the SEM image. Peaks in penetration depth plot indicate accumulation of debris during the test. Due to a partial elastic recovery after the test, metallic substrate is not readily visible from the SEM image; its damage has been assessed optically after the complete removal of the coating.

Coating thickness reaches a value of  $45.00 \pm 2.15 \mu\text{m}$ , computed based on scratch test results obtained from each sample, as explained in subSect. 2.4. Nevertheless, a low amount of variation occurs from one sample to another. To consider this factor, critical loads for cohesive and adhesive failure have been normalized for the estimated coating thickness of each sample.

Polished (P) and milled (M) coated samples show similar behavior and in the ending phase of testing coating is easily detached and raised from the substrates; milled ones perform

**Fig. 10** SEM image of a GB sample coated with chitosan/bioactive glass nanoparticles after scratch testing, different failure mechanisms are highlighted, and the representation is combined with load/penetration depth graphs plotted against tip displacement



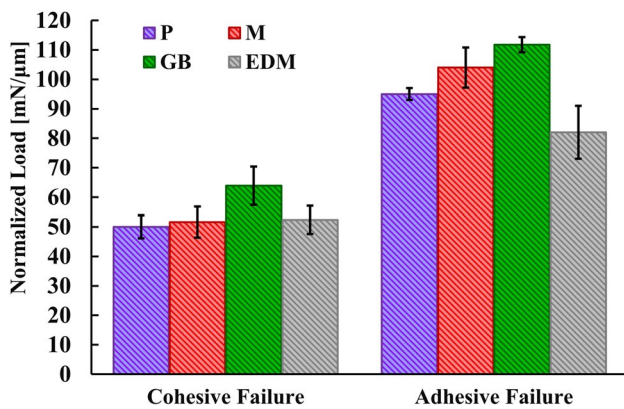


**Fig. 11** Critical scratch loads for different failure mechanisms of chitosan/bioactive glass nanoparticles coating, normalized to coating thickness. Reported error bars represent the standard deviation

better, due to the peculiar surface morphology of the process. The best case is represented by grit-blasted (GB), of which normalized critical loads exceed EDM by 36% and polished by 18% (Fig. 11). Also, coatings on P, M, and EDM samples were gradually completely detached from substrates under vacuum conditions required for SEM analysis, below  $2 \times 10^{-3}$  Pa. The same did not happen for GB samples.

## 4 Discussion

Ideally, cohesive failure, i.e., the onset of cracking of the coating, is expected to be unrelated to substrate surface characteristics; however, slight changes in coating thickness can lead to a change in the cohesive critical load. Also, the coating used herein was, by nature, inhomogeneous in terms of slight changes in bioactive glass particles distribution in the layer, causing possible variation in the cohesive failure.

Analyzing adhesive failure, the worst behavior is given by the presence of EDM-treated substrates as processing conditions bring the growth of a surface oxide layer with poor mechanical properties, resulting in multiple crack formation on both coating and substrate, indicating the unsuitability of the EDM process parameters to properly treat the samples for the specific application. This layer can be easily detached together with the coating, nullifying the effects of mechanical interlocking provided by the higher surface roughness and surface area. Also, the presence of residual stress in the chitosan-based coating layer, due to differences in thermal expansion with respect to substrate, might contribute to increasing the stress state in the tested area.

The improved behavior of GB samples can be due to a combination of factors. The grit blasting process was able to more effectively generate a surface prone to make intimate contact with the coating due to mechanical interlocking given by the peculiar surface topography and being demonstrated to

be effective in improving coating adhesion [14]. Also, scratch results partially follow the trend of contact angle values, having GB surfaces a good capability to be wetted by coating solution. Grit-blasting process, due to its easy and inexpensive implementation, has several upsides, and its combination with chemical etching can bring the generation of a well-performing surface but care should be taken in terms of the presence of debris from the blasting medium [27].

Polished samples exhibited a low adhesion strength as the poor chemical affinity of *Ti6Al4V* and the low surface energy usually displayed by the mirrored surface together with no mechanical interlocking effect lead to unsuccessful coating adhesion.

The overall results for milling and EDM show a slight increase in strength with respect to polishing, due to a more effective texturing of the surface. In fact, in both cases, mechanical texturing is the driving effect for the coating adhesion so that the delamination load is similar. However, the randomized texture obtained by grit blasting leads to better results since it allows to increase the energy needed for an open crack in the coating to propagate faster. In fact, grit blasted samples showed 18% and 36% higher normalized critical load with respect to polished and EDM treated samples, respectively.

## 5 Conclusions

The paper describes a methodology to improve *Ti6Al4V* surface quality with different mechanical and thermal surface processes to get a reliable chitosan-based coating. The overall treatments modified the surface roughness, topography, and chemical characteristics to a different extent influencing the coating adhesion probed via scratch test.

In particular, the tests demonstrated a strong influence of texture on adhesion parameters (contact angle, scratch test). The best performance is given by grit blasted substrates, while the others show markedly inferior coating adhesion.

The overall results contribute to the insight into surface modification of *Ti6Al4V* to improve coating performance by focusing on mechanical and thermal processes as the current state of the art does not allow to properly correlate adhesion and texture.

**Acknowledgements** The authors express their gratitude to Prof. Enrica Vernè and Dr. Marta Miola from Politecnico di Torino (Turin, Italy) for providing bioactive glass nanoparticles for the experimental campaign and Prof. Gerardo Catapano from Università della Calabria (Rende, Italy) for his support. The authors gratefully acknowledge Ing. Giuseppe Romeo from Meusbürger Georg GmbH & Co KG for providing technical support.

**Funding** Open access funding provided by Università della Calabria within the CRUI-CARE Agreement.

**Data availability** Not applicable.



**Code availability** Not applicable.

## Declarations

**Ethics approval** Not applicable.

**Consent to participate** Not applicable.

**Consent for publication** Not applicable.

**Conflict of interest** The authors declare no competing interests.

**Open Access** This article is licensed under a Creative Commons Attribution 4.0 International License, which permits use, sharing, adaptation, distribution and reproduction in any medium or format, as long as you give appropriate credit to the original author(s) and the source, provide a link to the Creative Commons licence, and indicate if changes were made. The images or other third party material in this article are included in the article's Creative Commons licence, unless indicated otherwise in a credit line to the material. If material is not included in the article's Creative Commons licence and your intended use is not permitted by statutory regulation or exceeds the permitted use, you will need to obtain permission directly from the copyright holder. To view a copy of this licence, visit <http://creativecommons.org/licenses/by/4.0/>.

## References

- Davis R, Singh A, Jackson MJ et al (2022) A comprehensive review on metallic implant biomaterials and their subtractive manufacturing. Springer, London
- Ratner BD, Hoffman AS, Schoen FJ, Lemons JE (2013) Biomater Science, 3rd edn. Academic Press
- Rehman MAU, Batool SA (2022) Development of sustainable antibacterial coatings based on electrophoretic deposition of multilayers: gentamicin-loaded chitosan/gelatin/bioactive glass deposition on PEEK/bioactive glass layer. *Int J Adv Manuf Technol* 120:3885–3900. <https://doi.org/10.1007/s00170-022-09024-3>
- Ramos Avilez HV, Castilla Casadiego DA, Vega Avila AL et al (2017) 11 -Production of chitosan coatings on metal and ceramic biomaterials. In: Amber Jennings J, Bumgardner JD (eds) Chitosan Based Biomaterials: Fundamentals, Volume 1. Woodhead Publishing, 255–293. <https://doi.org/10.1016/B978-0-08-100230-8.00011-X>
- Bumgardner JD, Wisner R, Gerard PD et al (2003) Chitosan: potential use as a bioactive coating for orthopaedic and craniofacial/dental implants. *J Biomater Sci Polym Ed* 14:423–438. <https://doi.org/10.1163/156856203766652048>
- Greene AH, Bumgardner JD, Yang Y et al (2008) Chitosan-coated stainless steel screws for fixation in contaminated fractures. *Clin Orthop Relat Res* 466:1699–1704. <https://doi.org/10.1007/s11999-008-0269-5>
- Sergi R, Bellucci D, Cannillo V (2020) A review of bioactive glass/natural polymer composites: state of the art. *Materials (Basel)* 13:1–38. <https://doi.org/10.3390/ma13235560>
- Rotella G, Alfano M, Candamano S (2015) Surface modification of Ti6Al4V alloy by pulsed Yb-laser irradiation for enhanced adhesive bonding. *CIRP Ann - Manuf Technol* 64:527–530. <https://doi.org/10.1016/j.cirp.2015.04.042>
- Seebach M, Fritz C, Kerschreiter J, Zaeh MF (2021) Shape accuracy and surface quality of additively manufactured, optimized, patient-specific bone plates. *J Med Devices Trans ASME* 15:1–7. <https://doi.org/10.1115/1.4049193>
- Jithin S, Joshi SS (2021) Surface topography generation and simulation in electrical discharge texturing: a review. *J Mater Process Technol* 298:117297. <https://doi.org/10.1016/j.jmatprotec.2021.117297>
- Samanta A, Wang Q, Shaw SK, Ding H (2020) Roles of chemistry modification for laser textured metal alloys to achieve extreme surface wetting behaviors. *Mater Des* 192. <https://doi.org/10.1016/j.matdes.2020.108744>
- Yumak N, Aslantas K (2020) A review on heat treatment efficiency in metastable b titanium alloys: the role of treatment process and parameters. *J Mater Res Technol* 9:15360–16280. <https://doi.org/10.1016/j.jmrt.2020.10.088>
- Jawahir IS, Brinksmeier E, M'Saoubi R et al (2011) Surface integrity in material removal processes: recent advances. *CIRP Ann - Manuf Technol* 60:603–626. <https://doi.org/10.1016/j.cirp.2011.05.002>
- Guo Y, Guan J, Peng H et al (2019) Tightly adhered silk fibroin coatings on Ti6Al4V biomaterials for improved wettability and compatible mechanical properties. *Mater Des* 175:107825. <https://doi.org/10.1016/j.matdes.2019.107825>
- Gupta V, Singh B, Mishra RK (2020) Machining of titanium and titanium alloys by electric discharge machining process: a review. *Int J Mach Mater* 22:99–121. <https://doi.org/10.1504/IJMMM.2020.105661>
- Lucca DA, Herrmann K, Klopstein MJ (2010) Nanoindentation: measuring methods and applications. *CIRP Ann - Manuf Technol* 59:803–819. <https://doi.org/10.1016/j.cirp.2010.05.009>
- Caridade SG, Merino EG, Alves NM et al (2013) Chitosan membranes containing micro or nano-size bioactive glass particles: evolution of biomineralization followed by in situ dynamic mechanical analysis. *J Mech Behav Biomed Mater* 20:173–183. <https://doi.org/10.1016/j.jmbbm.2012.11.012>
- Mota J, Yu N, Caridade SG et al (2012) Chitosan/bioactive glass nanoparticle composite membranes for periodontal regeneration. *Acta Biomater* 8:4173–4180. <https://doi.org/10.1016/j.actbio.2012.06.040>
- Caridade SG, Merino EG, Luz GM et al (2010) Bioactivity and viscoelastic characterization in physiological simulated conditions of chitosan/Bioglass® composite membranes. *Mater Sci Forum* 636–637:26–30. <https://doi.org/10.4028/www.scientific.net/MSF.636-637.26>
- Barnes D, Johnson S, Snell R, Best S (2012) Using scratch testing to measure the adhesion strength of calcium phosphate coatings applied to poly(carbonate urethane) substrates. *J Mech Behav Biomed Mater* 6:128–138. <https://doi.org/10.1016/j.jmbbm.2011.10.010>
- ASTM International (2020) ASTM D7027–20 — standard test method for evaluation of scratch resistance of polymeric coatings and plastics using an instrumented scratch machine. <https://doi.org/10.1520/D7027-20>
- Mishra SK, Kannan S (2014) Development, mechanical evaluation and surface characteristics of chitosan/polyvinyl alcohol based polymer composite coatings on titanium metal. *J Mech Behav Biomed Mater* 40:314–324. <https://doi.org/10.1016/j.jmbbm.2014.08.014>
- Frank O, Zuckalova M, Laskova B et al (2012) Raman spectra of titanium dioxide (anatase, rutile) with identified oxygen isotopes (16, 17, 18). *Phys Chem Phys* 14:14567–14572. <https://doi.org/10.1039/c2cp42763j>
- Krishnan SV, Palanivelu S, Ambalam MMM et al (2018) Chemical synthesis and characterization of nano alumina, nano composite of carbon-alumina and their comparative studies. *Zeitschrift fur Phys Chemie* 232:1827–1842. <https://doi.org/10.1515/zpch-2017-1075>
- Aminzadeh A (1997) Excitation frequency dependence and fluorescence in the Raman spectra of Al<sub>2</sub>O<sub>3</sub>. *Appl Spectrosc* 51:817–819. <https://doi.org/10.1366/0003702971941331>
- Rahman SS, Ashraf MZI, Bashar MS et al (2017) Crystallinity, surface morphology, and chemical composition of the recast layer and rutile-TiO<sub>2</sub> formation on Ti-6Al-4V ELI by wire-EDM to enhance biocompatibility. *Int J Adv Manuf Technol* 93:3285–3296. <https://doi.org/10.1007/s00170-017-0772-5>
- Brunette DM, Tengvall P, Textor M, Thomsen P (2001) Titanium in medicine: material science, surface science, engineering, biological responses and medical applications. Springer-Verlag Berlin Heidelberg GmbH

**Publisher's note** Springer Nature remains neutral with regard to jurisdictional claims in published maps and institutional affiliations.